Russian Journal of Earth Sciences, Vol. 22, ES6012
https://doi.org/10.2205/2022ES000825

Wavelet analysis of geomagnetically induced currents during the strong geomagnetic storms

T. V. Aksenovich*[,1], V. A. Bilin[1,2], Ya. A. Sakharov[1,2], and V. N. Selivanov[1]

[1] *Northern Energetics Research Centre – Branch of the Federal Research Centre "Kola Science Centre of the Russian Academy of Sciences", Apatity, Murmansk region, Russia*
[2] *Polar Geophysical Institute, Apatity, Murmansk region, Russia*

Received 12 July 2022; accepted 20 December 2022; published 31 December 2022.

The main problem of electric utilities around the world is to ensure continuous power supply to consumers. One of the causes of power outages and blackouts can be geomagnetic storms during periods of the increased solar activity. They arouse geomagnetically induced currents (GICs) flowing in the long-distance high-voltage power grids on Earth's surface. The history of this phenomenon investigation shows that GICs during strong geomagnetic storms had led to blackouts in certain regions of Canada, Sweden and the USA. To study these phenomena and assess the risks of such accidents for the regional system, a GICs registration system in 330 kV autotransformers neutrals of the Kola-Karelian power transit was developed in northwestern Russia. During 11 years of monitoring numerous cases of the flow of high values of quasi-DC currents with different time durations, induced by variations of the geomagnetic field, have been registered. In order to analyze the currents a wavelet transform was chosen, since this method allows to define not only the frequency composition but also changes in spectral characteristics over time, which is significant in the study of GIC. The paper presents a discussion of GIC scalograms obtained for four events of Solar Cycle 24: 13–14 November 2012, 17–18 March 2015, 7–8 September 2015 and 7–8 September 2017. The analysis showed that the characteristic duration of the peak of the considered GICs is from 4.6 to 11.1 min.

Keywords: geomagnetically induced currents, geomagnetic storm, autotransformer, continuous wavelet transform

Citation: Aksenovich, T. V., V. A. Bilin, Ya. A. Sakharov, and V. N. Selivanov, (2022), Wavelet analysis of geomagnetically induced currents during the strong geomagnetic storms, *Russian Journal of Earth Sciences*, Vol. 22, ES6012, doi: 10.2205/2022ES000825.

1 Introduction

The Sun is a starting point of a creation chain of geomagnetically induced currents (GICs) in technological systems on Earth. During the periods of the increased solar activity, events on the Sun's surface, such as coronal mass ejections (CME) and solar flares, occur. These phenomena are accompanied by eruption of a large number of charged particles, which form high-speed solar wind. If the stream of charged particles is aimed to our planet, then the plasma energy is transferred into the magnetosphere, as the result of the interaction between solar wind and Earth's magnetic field. In the magnetosphere this energy is accumulated and released in the form of strong geomagnetic disturbances (GMDs). The process of such interaction is called a geomagnetic storm.

During geomagnetic storm significant changes in currents and fields of Earth's magnetosphere occur, which induce geoelectric field at its surface and in the ground. The field causes a flow of GICs in the earthed utility systems, such as power grids [*Belakhovsky et al.*, 2019; *Boteler*, 2001; *Erinmez et al.*, 2002; *Liu et al.*, 2009]. The best-known examples of the GIC impact on power systems are an outage of Hydro-Québec electricity transmission system in Canada on 13 March 1989 [*Guillon et al.*, 2016] and a blackout of the high-voltage power system in southern Sweden on 30 October 2003 [*Pulkkinen et al.*, 2005].

*Corresponding author: t.aksenovich@ksc.ru

Geoelectric field values for strong GMDs range from 1 to 10 V km^{-1} typically [*Pulkkinen et al.*, 2008]. In this case GICs values can constitute tens and in some cases hundreds of amperes. The largest GIC value, which equals to almost 300 A, was measured in a 400 kV transformer neutral in southern Sweden during the magnetic storm on 6 April 2000 [*Wik et al.*, 2008].

GIC is often referred to as quasi-DC current. This is due to the fact that it has a frequency range between 1 and 100 mHz compared to the ac power system frequency of 50 or 60 Hz. Therefore, GIC can be considered as almost constant (quasi-DC) current. Flowing through "the ground – neutral wire of transformer – windings of transformer – wires of power transmission lines – windings of transformer – neutral wire of transformer – the ground" circuit, the quasi-DC current may result in a number of disruptions of electrical networks operation, while the duration of its impact often doesn't exceed a few minutes.

The most vulnerable component of the power system for GIC impact is a power transformer. Increase of quasi-DC currents level (tens of amperes) in transformer neutral leads to half-cycle saturation of the transformer core. This causes some detrimental effects on power system operation such as increase of reactive power consumption, generation of even and odd harmonics, appearance of local overheating of transformer windings and elements of its construction [*Kappenman*, 2018; *Molinski*, 2002]. Long-term effects of GICs can result in significant damage to the transformer due to cumulative effect.

In recent times, researchers involved in the study of geomagnetically induced currents began to apply spectral analysis techniques more frequently [*Adhikari et al.*, 2019; *Falayi et al.*, 2017; *Xu et al.*, 2022]. The wavelet analysis method is the most commonly utilized method for spectral processing of quasi-DC currents. The main advantage of the wavelet transform (WT) is to identify non-stationary signals, which include GICs too. Selecting the appropriate wavelet function type and varying its parameters allows WT to achieve the most accurate determination of time localization of different frequency components of signal in the best way.

It was noted in research [*Falayi et al.*, 2017] that geomagnetic storms, which are accompanied by significant geomagnetic disturbances, are featured by high values of wavelet coefficients in most cases. This relation is clearly visible on the obtained wavelet spectra of GIC data. The authors used the Morlet wavelet as the mother wavelet. In the article [*Adhikari et al.*, 2019] continuous wavelet transform (CWT) is applied to find the variability and periodicity associated with GIC in the pipeline. This research showed that the GIC signal has a highly variable nature with time. It was also found that higher intensity of average energy is observed during events with higher GIC values, i.e. wavelet spectra coefficients and GIC values are related. There is no information about the used analyzing function. Besides that, authors in [*Xu et al.*, 2022] used spectra of CWT to gain greater insight into a relation between GIC and horizontal component of geomagnetic field *dBx/dt* during the intense geomagnetic storm. The research showed that GIC and *dBx/dt* data have a certain correlation between them. The non-orthogonal Morlet wavelet was chosen as the wavelet function.

The main focus of this paper is to study quasi-DC currents in autotransformers by using wavelet transform method to specify their spectral characteristics. The analysis of the GIC scalograms showed that the frequency range of the considered GICs is 1.5–3.6 mHz.

The structure of the paper is as follows. In section 2, we describe the data used in this study and the method of wavelet analysis. The subsection 2.1 deals with a brief discussion of the registration system of GMDs in power grids in northwestern Russia and sampling rate of GIC data. In subsection 2.2, we give main information about continuous wavelet transform. In subsection 2.3, we explain the choice of mother wavelet type for wavelet transform of GICs measurements. Section 3 reports the wavelet spectra of GICs at two substations of the monitoring system and detailed analysis and comparison of them for four geomagnetic storms of Solar Cycle 24. Finally, we discuss and summarize our study in section 4.

2 Data and the analysis method

2.1 Brief information about geomagnetically induced currents monitoring system

The GIC data used in the current study are obtained from a system for monitoring GICs in power lines in northwestern Russia [*Barannik et al.*, 2012]. This system was developed by the Polar Geophysical Institute (Russian Academy of Sciences) and the Northern Energetics Research Centre (Kola Science Centre of the Russian Academy of Sciences) in the frameworks of the European Risk from Geomagnetically Induced Currents (EURISGIC) project in 2011 [*Viljanen*, 2011]. It was deployed on the Kola Peninsula and in Karelia and consists of 5 substations, located in the meridional direction, as shown in Figure 1.

The devices at VKH, TTN, LKH and KND substations installed in the dead-grounded neutral of 330 kV autotransformers, and in the neutral of 110 kV transformer at the RVD substation. The to-

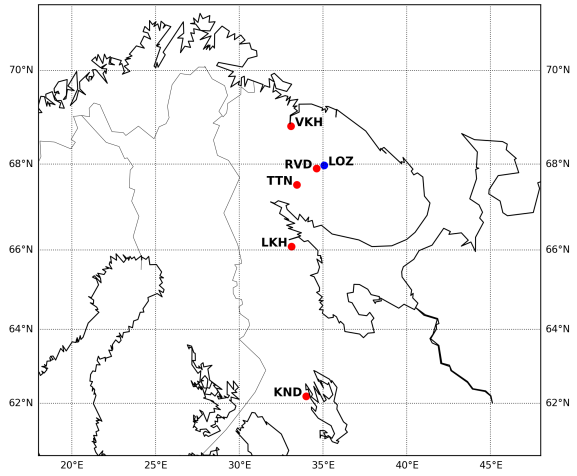

Figure 1: A map of the network of GIC monitoring devices (red dots) at substations in northwestern Russia and LOZ magnetometer station (blue dot).

tal current in the network node is twice the measured value, because probes are located on one of the two step-down autotransformers at a substation, with the exception of the KND substation.

The GIC monitoring device consists of three main parts [*Barannik et al.*, 2012]:

1. clamp-type current sensor using Hall element (the measurement range is ±200 A and the frequency range is 0–400 Hz);
2. data processing unit (the microcontroller performs analog-to-digital conversion of the input signal with a sampling rate at 10 Hz for further data processing);
3. unit for storing and transmitting data to the server.

Measurements are carried out continuously by most devices of the monitoring system to the present. Information about coordinates of GIC monitoring points and availability of measurements data for each substation is listed in Table 1. Current and archived GIC monitoring data and data of magnetic observations at geophysical observatories in the region are available on the website (http://eurisgic.ru/). The information is presented in the form of overview graphs. The sampling interval of GIC observations presented on the website is 1 min, which is sufficient for a preliminary assessment of the GIC presence in the neutral current.

In this study we use 1 s GIC data, i.e. the sampling rate is 1 Hz. In research devoted to analysis of the effect of GIC observations sampling rate on its peak values and time localization was found that the increase of sampling interval to 10 s and even 1 min leads to underestimation of peak values of GIC (decrease to 10 A), shifts in peak values timing and omissions of some GIC values in range of 40–70 A [*Trichtchenko*, 2021]. This in turn may negatively affect the validity of subsequent experiments, which will use data with such sampling rates. Based on the above conclusions and computational efficiency, it was decided to use 1 s GIC data for the analysis.

Due to the potential hazard that GIC poses to the operation of continuously expanding power systems around the world, monitoring systems such as that described above have been established in several countries [*Albert et al.*, 2022; *Choi et al.*, 2015; *Mac Manus et al.*, 2017; *Watari et al.*, 2021]. The key features of the geomagnetic disturbances monitoring system in northwestern Russia include long-term continuous recording of GIC (more than 10 years), high sampling rate equal to 10 Hz (0.1 s) and high-latitude location of monitoring stations.

2.2 Continuous wavelet transform

The wavelet transform is a well-known technique used to analyze the spectra of various non-stationary signals in many areas of science. There are two types of wavelet transform: continuous wavelet transform and discrete wavelet transform. We selected the first one to study GIC signal in the autotransformer neutral, because it provides insight into the signal frequency content with respect to time.

The main idea of the CWT is to estimate a cross correlation of an analyzed signal with a set of wavelets of various "widths" ("scales") at different time positions. The wavelet coefficients are the result of the comparison of these signals. The greater

Table 1: Information about the GIC monitoring network in northwestern Russia

Substation		Geographical coordinates		The period of registration
Code	Name	Latitude (°N)	Longitude (°E)	
VKH	Vykhodnoy	68.83	33.08	October 2011 – until now
RVD	Revda	67.90	34.61	June 2006 – until now
TTN	Titan	67.53	33.44	June 2010 – May 2015
LKH	Loukhi	66.08	33.12	June 2011 – until now
KND	Kondopoga	62.22	34.36	June 2011 – until now

the coefficient value, the more the signals are similar to each over. The set of wavelets is obtained by scaling and translating the mother wavelet. Mathematically, the continuous wavelet transform of a discrete time series x_n is given by [*Torrence and Compo*, 1998]:

$$W_n(s) = \sum_{n'=0}^{N-1} x_{n'} \psi^* \left[\frac{(n'-n)\,\delta t}{s} \right],$$

where n is the localized time index, s is the wavelet scaling factor, ψ is the mother wavelet, the (*) denotes the complex conjugate and δt is equal time spacing.

Wavelets are referred to as the mathematical functions, which most frequently have the form of waves and their range of variability tends to zero with distance from the origin of coordinates. Wavelets are localized in time and frequency, which makes it possible to obtain frequency spectrum features of a signal with respect to time. Since the appearance of the wavelet analysis method, a large number of analyzing functions – mother wavelets – has been created. This is justified by the fact that different mother wavelets have different properties and give different results when applied to the same signal, respectively.

The CWT result is a three-dimensional array of wavelet coefficients $W_n(s)$. The graphical representation of the CWT result is a scalogram: the x axis indicates time, the y axis represents a frequency whose value is inversely proportional to the wavelet scale, and colors indicate the wavelet coefficients values which characterize the "similarity" degree between the analyzed signal and the wavelet. The scalogram is an equivalent of the spectrogram of the Short-time Fourier transform (STFT) and it's calculated as the square of the modulus of the wavelet coefficients values $|W_n(s)|^2$.

The CWT has several advantages in the analysis of non-stationary signals over the STFT. In the previous study [*Aksenovich*, 2020], the comparison of the application of these spectral analysis methods of signals to the current in autotransformer neutral was made. It showed that the CWT is better suited for the detection of GIC than the STFT. For example, it gives more accurate and informative results about the local features of the signal. In addition, the use of wavelets (instead of sinusoids in the STFT) allows the CWT to achieve good localization in the frequency domain and maintain sufficient quality in the time domain at the same time. It is reached through two distinctive properties of the CWT. First, the wavelet function can have different shapes, whereas only a sinusoid is used in the STFT. Second, the original wavelet is scaled during the analysis, i.e. it is shrunk and stretched, while the window size is still constant during the STFT. High time-frequency resolution is very important to accurately determine the time and duration of the GICs in the neutral.

2.3 Wavelet transform parameters

As mentioned above in subsection 2.2, there are wavelet functions that have different properties and are suitable for solving different problems. In this paper we use open source library PyWavelets, which serves, in particular, to compute the CWT [*Lee et al.*, 2019]. The library contains the following families of CWT compatible mother wavelets: Mexican Hat wavelet ("mexh"), Morlet wavelet ("morl"), Complex Morlet wavelets ("cmorB-C"), Gaussian Derivative wavelets ("gausP"), Complex Gaussian Derivative wavelets ("cgauP"), Shannon wavelets ("shanB-C") and Frequency B-spline wavelets ("fbspM-B-C"). Where B, C, P and M is the wavelet bandwidth, center frequency, P-th order derivative of the function and spline order, respectively.

The Morlet wavelet is considered to be the most suitable wavelet for problems of the bursts of energy release. This is explained by the fact that it meets the requirement of exact equality in the Heisenberg relation, which specifies the uncertainties in the time and frequency localization of studied bursts [*Mallat*, 2008]. The application of CWT to obtain GIC scalograms has not widely disseminated yet, and, consequently, has no specific parameters of the analyzing function. Based on this, it was decided to verify adequacy of using the Morlet wavelet for the analysis of quasi-DC currents in the neutral of an autotransformer in practice.

Seven GIC scalograms for mother wavelets listed above were analyzed with an example of the event of 7 September 2017 (Figure 2). Comparison of the obtained scalograms showed that the "morl" (Figure 2a) and "gaus8" (Figure 2d) wavelet functions give the most accurate time-frequency representation of GIC signal in the neutral current. Their spectra are similar to each over: both scalograms have distinct peaks in time at approximately equal frequencies. Nevertheless, the number of apparent peaks is larger for the Morlet wavelet, and they do not tend to shift to the y axis. In addition, a computation time of the coefficients for both wavelets was compared. The comparison showed that the speed of the CWT coefficients computation is higher for the "gaus8" wavelet function. Since the main aim of the study is to accurately determine the values of the GIC frequencies and time of its presence in signal, the Morlet wavelet was chosen for further analysis, taking into account the above facts. In this context, the computational speed can be neglected in favor of greater accuracy of the determination of the wavelet coefficients values. The Morlet wavelet was also previously used by other

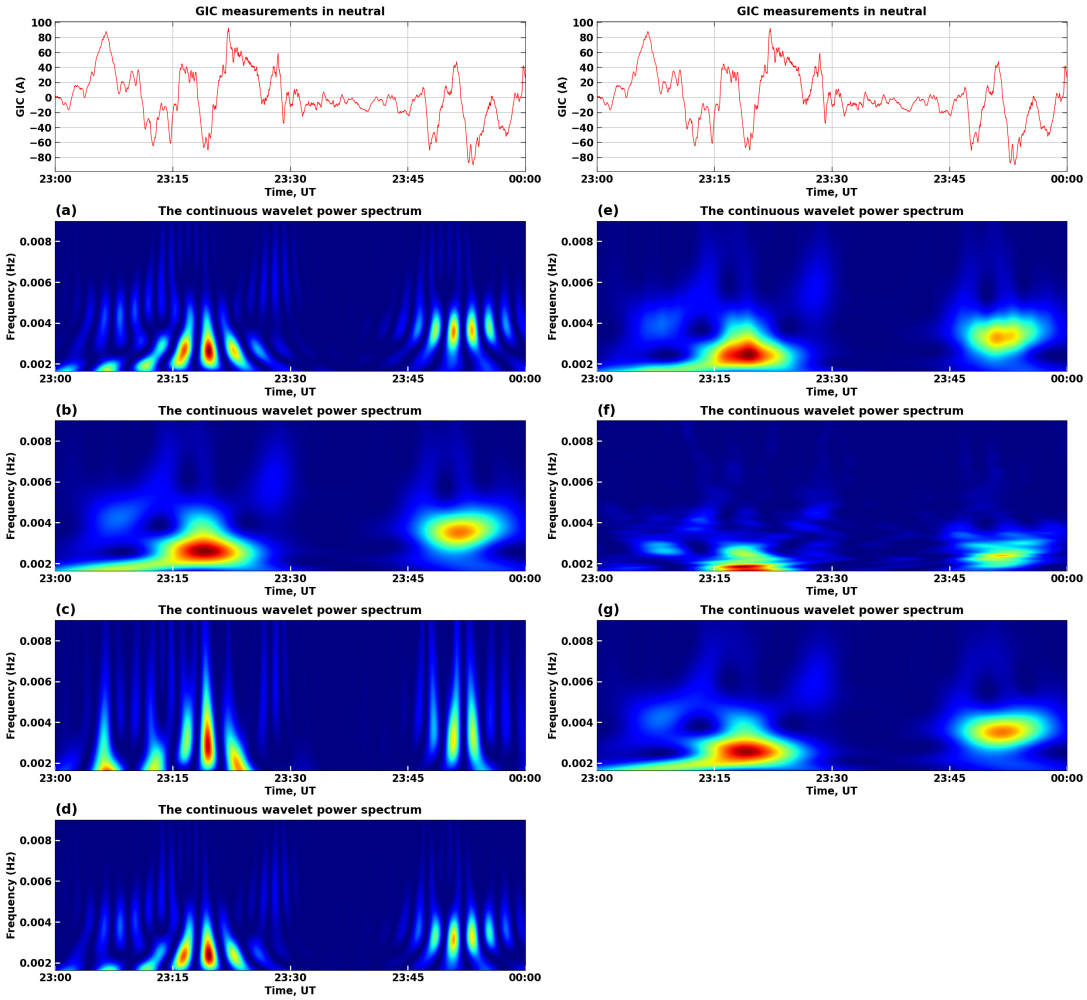

Figure 2: Continuous wavelet transforms of GIC signal, using: a) Morlet wavelet; b) Complex Morlet wavelet with B = 1.8 and C = 0.8; c) Mexican Hat wavelet; d) Gaussian Derivative wavelet with P = 8; e) Complex Gaussian Derivative wavelet with P = 8; f) Shannon wavelet with B = 0.6 and C = 0.9; g) Frequency B-spline wavelet with M = 4, B = 1.0 and C = 0.8.

researchers to calculate the GIC wavelet spectra [*Falayi et al.*, 2017; *Xu et al.*, 2022]. The rest of the mother wavelets in Figure 2 are not useful for the purpose of the study because of blurry localization of the coefficients in the time (Figure 2b, Figure 2e, Figure 2g) and frequency (Figure 2c) domains and the presence of artifacts (Figure 2f), which do not provide a clear picture of the spectral characteristics of the processes in the neutral current.

3 Wavelet transform view of the geomagnetically induced currents fluctuations

The GIC monitoring system in high-voltage power lines is located in northwestern Russia. In particular, the recording devices are installed at the substations of the Murmansk region (VKH, RVD, TTN) and in Karelia (LKH, KND). During Solar Cycle 24, which lasted from December 2008 to December 2019, no accidents caused by space weather were recorded in the power systems of these regions. However, the devices of the monitoring system registered several cases of GICs flow, the values of which were exceeded by several times the threshold of the normal value of the current in the autotransformer neutral on geomagnetically quiet days.

In this article we will carry out wavelet analysis of data from two substations of the system – VKH and LKH. Selection of these points is justified by the fact that the data of these substations almost completely cover the time period of Solar Cycle 24 and both substations are through ones. It should be noted that at the VKH substation, unlike LKH, the lines change their direction from meridional to latitudinal. This topological feature can influence the GIC value in the neutral towards its increase, which will be further highlighted in the paper. During the observation period it was found that

Table 2: Dates of the Solar Cycle 24 events with high GICs at VKH and LKH substations

Number	Dates	Maximum Currents, A	
		VKH	LKH
1	12 June 2012	62.46	4.51
2	13–14 November 2012	39.37	4.99
3	27 March 2013	62.82	6.34
4	1 June 2013	51.60	5.45
5	17–18 March 2015	72.86	6.14
6	7–8 September 2015	51.08	54.57
7	2 September 2016	94.38	6.36
8	7–8 September 2017	92.26	31.52

the average level of the current in the autotransformer neutral at the time of relatively low geomagnetic activity does not exceed 2 A and 1 A in absolute value for VKH and LKH substations, respectively. Depending on the mode of operation of the power system, these values may vary slightly.

Brief information about geomagnetic storms of Solar Cycle 24 that caused the flow of high values GICs is summarized in Table 2. Of all the events, four were selected for further wavelet analysis: 13–14 November 2012, 17–18 March 2015, 7–8 September 2015 and 7–8 September 2017. One common feature of all these events is that geomagnetic storms on these dates were associated with CMEs [*Dimmock et al.*, 2019; *Watari*, 2017; *Wu et al.*, 2016].

We will begin our analysis with the event of 7–8 September 2015, when the maximum values of GICs at both substations were almost equal. So assuming that during the magnetic storm all overhead lines of the Kola-Karelian power transit are located in the area of spatially homogeneous disturbance of the geomagnetic field. In the normal mode of operation of the electrical network, when all power lines and autotransformers operate, GICs at the VKH substation are approximately an order of magnitude higher than those at the LKH substation. This is due to the topology of the electrical network and orientation of power lines relative to the disturbance vector of the horizontal component of the geomagnetic field. If power lines, which are directed from and to through substation, do not globally change their direction (as at LKH and KND substations and at other through substations of the Kola-Karelian power transit), then input and output GICs in autotransformer neutral compensate each other. In this case, the resulting currents have low values. At the VKH substation, lines change their direction from meridional to latitudinal. GICs are usually differed significantly in perpendicular lines due to the difference in the "active" components of the geomagnetic field. This leads to high values of the resulting GICs in the autotransformer neutral. During the event of 7–8 September 2015, the outgoing overhead line, which is directed to the south from the LKH substation, was disconnected, for this reason only current from the overhead line coming from the north flowed in the autotransformer neutral. This explains the high current value at the LKH substation. And the equality of currents at VKH and LKH substations is a consequence of the spatial homogeneity of the GMD over the territory of the Kola-Karelian power transit.

To determine the qualitative relation between GICs at selected substations and geomagnetic field disturbances at LOZ magnetometer station, a wavelet analysis of the first time derivative of the geomagnetic component *dBy/dt* was additionally carried out. Studies show that there is a high correlation between the GIC values at Kola-Karelian power transit substations and variations of geomagnetic field, which has an east-west direction [*Yagova et al.*, 2021]. In the general case, the response evaluation of a distributed and partially grounded power system to an alternating magnetic field of a magnetospheric disturbance requires a fairly complex analysis of transfer functions with multiple inputs. It is required to know the impedance distribution in the area of line location as well [*Oliveira and Ngwira*, 2017]. In this work, we have posed another problem, which is to determine the qualitative relation between the quasi-DC current recorded in the electric power system and changes in the geomagnetic field.

Cross-correlation coefficients were calculated between the derivatives of horizontal components of the geomagnetic field *dBx/dt* and *dBy/dt* and the GIC value at the VKH substation for the event 7–8 September 2015. The relationship between GIC and *dBy/dt* ($r = 0.42$) turned out to be much closer than between GIC and *dBx/dt* ($r = -0.03$). In this case, the GIC at the selected substations can be fully determined by the nature of auroral current disturbance, which has a north-south direction.

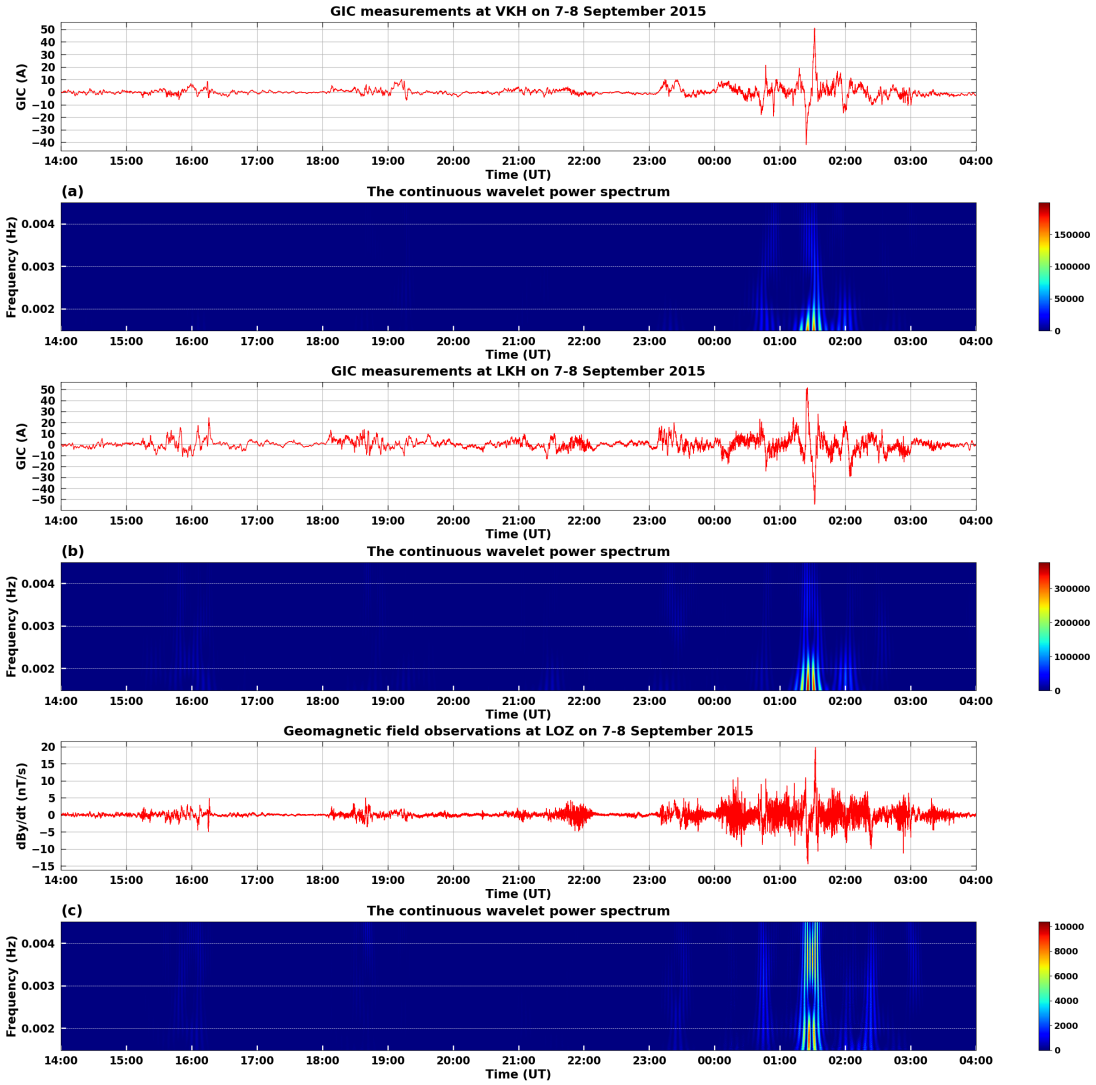

Figure 3: Geomagnetically induced currents at VKH and LKH substations and geomagnetic field observations at LOZ station during geomagnetic storm on 7–8 September 2015: a) wavelet power spectrum of current at VKH; b) wavelet power spectrum of the current at LKH; c) wavelet power spectrum of dBy/dt at LOZ.

Thus, setting the aim of determining the qualitative relation between the quasi-DC current recorded in the electric power system and changes in the geomagnetic field using the wavelet spectrum of the signal, it was decided to limit consideration to one component of the geomagnetic field and the qualitative comparison of the signal spectra.

Figure 3 shows GICs signals and the first time derivative of the geomagnetic component dBy/dt, as well as the corresponding wavelet power spectra (Figure 3a, b and c) at VKH and LKH substations and at LOZ magnetometer station from 7 to 8 September 2015. Hereinafter the color shows the intensity of the wavelet coefficients, where red corresponds to the maximum value of the energy, and blue corresponds to the minimum one. The CWT coefficient value is directly proportional to the degree of coincidence of the shape of the scaled mother wavelet with the shape of the studied signal. During the geomagnetic storm on 7–8 September 2015, the increase in the GIC amplitudes was observed in the region from 15:00 UT to 04:00 UT at both substations. For the VKH substation, the highest values of wavelet coefficients were obtained from 01:00 UT to 02:00 UT at a frequency of 1.5 mHz, which corresponds to a time scale of ~11.1 min. For the LKH substation, the highest values of wavelet coefficients also had one peak from 01:00 UT to 02:00 UT at a frequency of 1.6 mHz (~10.4 min). The peaks of spectra energy coincide in time at both substations. On the scalogram of the time derivative of the geomagnetic field component By (Figure 3c), the highest values of wavelet coefficients also had a peak in the region from 01:00 UT to 02:00 UT at a frequency

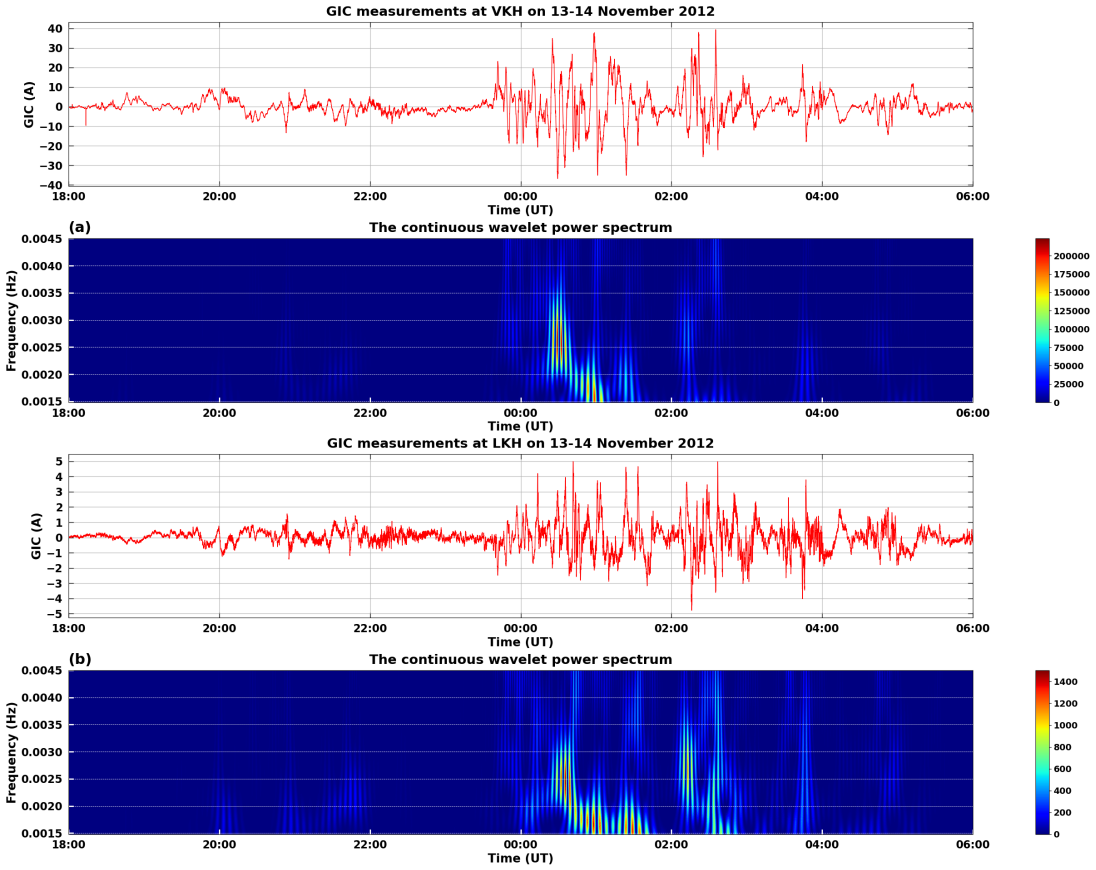

Figure 4: Geomagnetically induced currents at VKH and LKH substations during geomagnetic storm on 13–14 November 2012: a) wavelet power spectrum of the current at VKH; b) wavelet power spectrum of the current at LKH.

of 1.8 mHz (~9.3 min) and 3.7 mHz (~4.5 min). The last frequency is high-frequency noise, which is caused by the processing method of data from LOZ magnetometer station. The frequency does not affect the fluctuations of the GIC signal at the considered substations.

As can be seen from Figure 3a and Figure 3b, there are no GIC signals with a constant frequency on the scalograms. The frequencies values of observed quasi-DC currents practically do not change and vary in a narrow range of 1.5 to 1.6 mHz (11.1 and 10.4 min, respectively). The spectra energy is in good agreement with GICs fluctuations.

Figure 4 shows GICs signals and the corresponding wavelet power spectra (Figure 4a and Figure 4b) at VKH and LKH substations during the period from 13 to 14 November 2012. The GIC fluctuations were observed between the period 18:00 UT and 06:00 UT at both substations. For the VKH substation, the highest values of wavelet coefficients were obtained from 00:00 UT to 01:00 UT at a frequency of 2.6 mHz, which corresponds to a time scale of ~6.4 min. For the LKH substation, the highest values of wavelet coefficients had two peaks during the period from 00:00 UT to 01:00 UT at a frequency of 2.5 mHz (~6.7 min) and from 02:00 UT to 02:30 UT at a frequency of 2.7 mHz (~6.2 min). At the VKH substation, the second peak from 02:00 UT to 02:30 UT did not cause such a significant response in the spectrum.

As well as scalograms in Figure 3a and Figure 3b, the scalograms (Figure 4a, Figure 4b) do not contain GIC signals with a constant frequency. The frequencies values of observed quasi-DC currents vary in a range of 2.5 to 2.7 mHz (6.7 and 6.2 min, respectively). The spectra energy corresponds well to the GICs fluctuations. At the same time, the GIC values that are within 10 A practically did not affect the scalogram at the VKH substation, in contrast to the GIC at the LKH substation, which is equal to ~2 A. This may be due to the fact that the values of wavelet coefficients for VKH are tens of times higher than the coefficients values for LKH. Therefore, in further research, parts of a signal with high and medium GICs should be analyzed separately.

Figure 5 represents GICs signals and the corresponding wavelet power spectra (Figure 5a and Figure 5b) at VKH and LKH during 17–18 March 2015. An increase in the GIC amplitudes was observed in the region from 20:15 UT to 01:00 UT

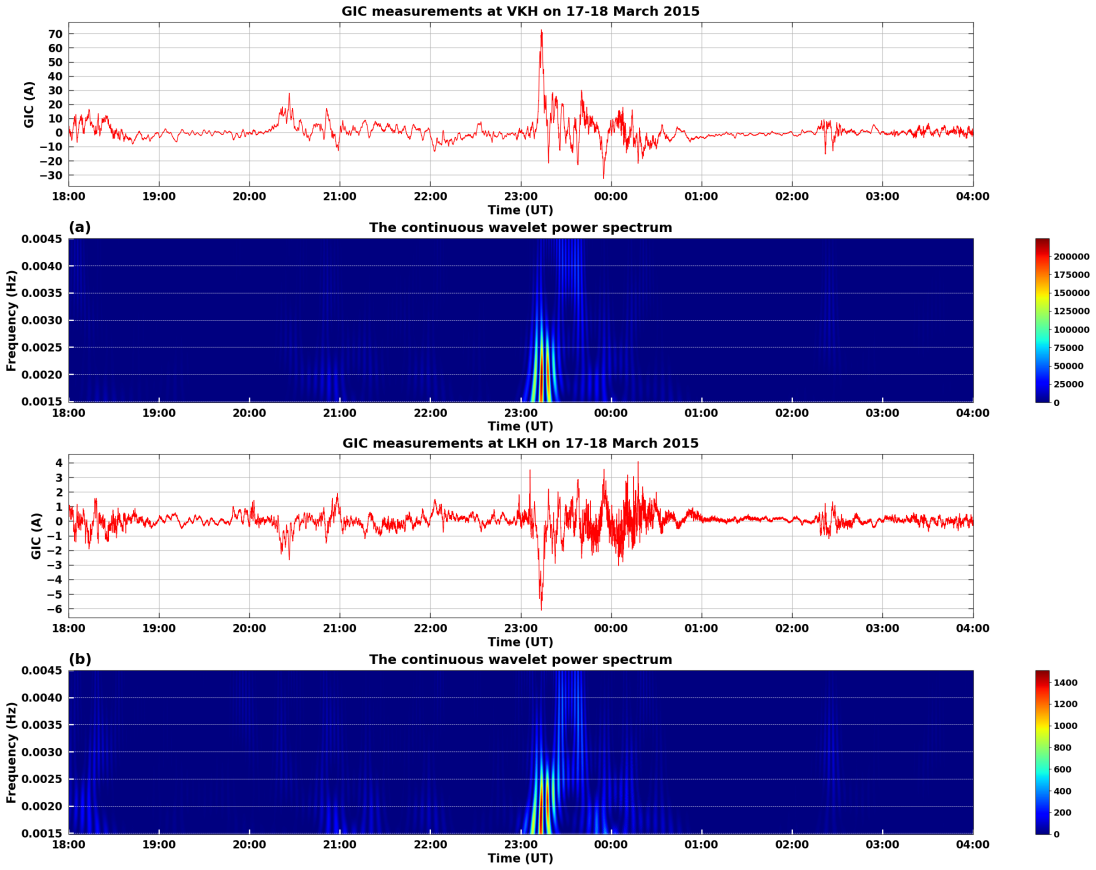

Figure 5: Geomagnetically induced currents at VKH and LKH substations during geomagnetic storm on 17–18 March 2015: a) wavelet power spectrum of the current at VKH; b) wavelet power spectrum of the current at LKH.

at VKH and from 20:15 UT to 00:15 UT at LKH. For the VKH substation, the highest values of wavelet coefficients were obtained from 23:00 UT to 23:30 UT at a frequency of 2.0 mHz, which corresponds to a time scale of ~8.3 min. For the LKH substation, the highest values of wavelet coefficients also had one peak during the period from 23:00 UT to 23:30 UT at a frequency of 1.9 mHz (~8.8 min). The peaks of spectra energy coincide in time at both substations.

As can be seen from Figure 5a and Figure 5b, there are no GIC signals with a constant frequency on the scalograms. The energy of the spectra is greater for high amplitudes of GIC fluctuations than for low ones. During this geomagnetic storm, the GIC frequencies varied in a narrow range of 1.9 to 2.0 mHz (8.8 and 8.3 min, respectively). Fluctuations with low amplitudes are observed on both scalograms (at 20:15–22:15 UT).

Figure 6 shows GIC fluctuations and results of their CWT (Figure 6a and Figure 6b) at VKH and LKH substations during geomagnetic storm on 7–8 September 2017. An increase in the GIC amplitudes was observed in the region from 22:00 UT to 03:00 UT at VKH and from 23:00 UT to 03:00 UT at LKH. For the VKH substation, the highest values of wavelet coefficients were obtained from 23:00 UT to 23:30 UT at a frequency of 2.6 mHz, which corresponds to a time scale of ~6.4 min, and from 23:45 UT to 00:00 UT at a frequency of 3.6 mHz, which corresponds to a time scale of ~4.6 min. For the LKH substation, the highest values of wavelet coefficients had two peaks during the period from 23:45 UT to 00:00 UT at a frequency of 3.5 mHz (~4.8 min) and from 01:00 UT to 01:30 UT at a frequency of 2.0 mHz (~8.3 min). The peaks of spectra energy partially coincide in time at both substations.

The scalograms (Figure 6a and Figure 6b) do not contain GIC signals with a constant frequency. The frequencies values of observed quasi-DC currents vary in a range of 2.0 to 3.6 mHz (8.3 and 4.6 min, respectively). The spectra energy is in good agreement with GICs fluctuations. Between the period from 01:00 UT to 02:00 UT, GIC fluctuations with amplitudes about 20 A were practically not reflected on the VKH scalogram, while similar values led to peak values of wavelet coefficients in the same region on the LKH scalogram. This difference can be explained by the fact that the values of wavelet coefficients for VKH are tens of times higher than the coefficients values for LKH.

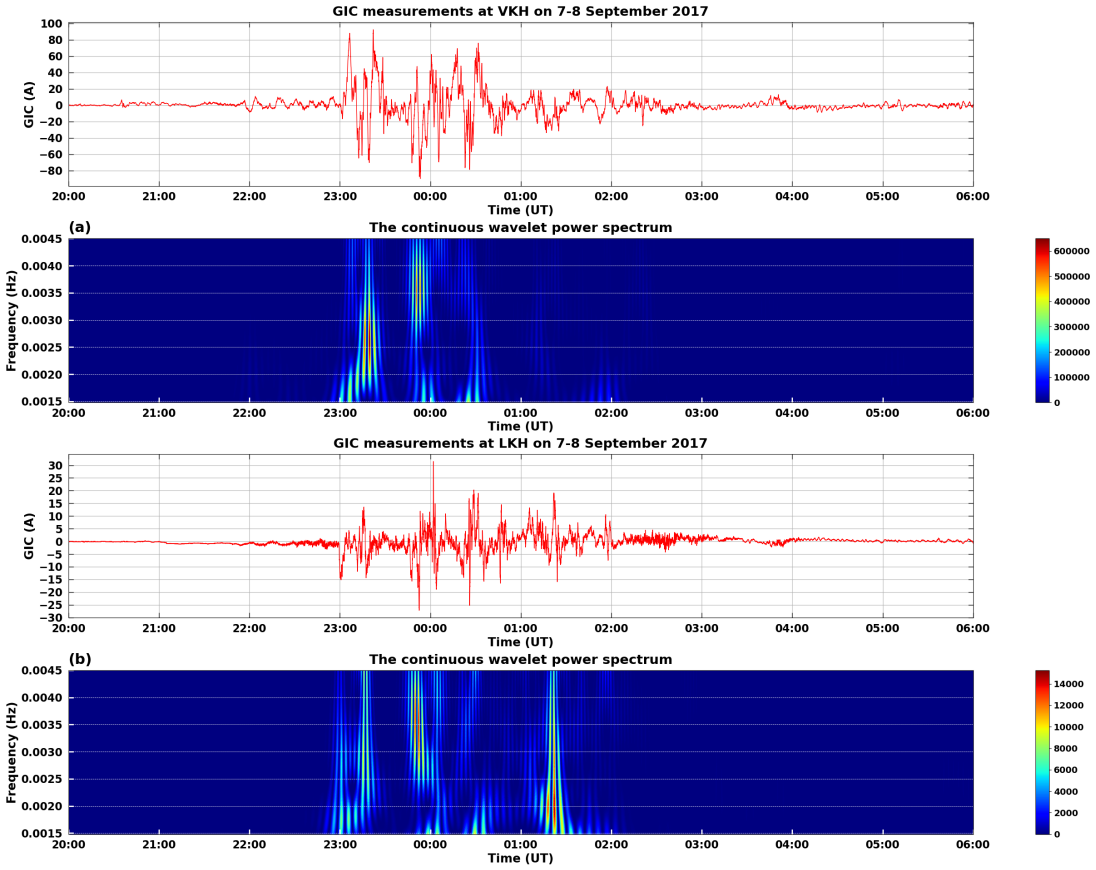

Figure 6: Geomagnetically induced currents at VKH and LKH substations during geomagnetic storm on 7–8 September 2017: a) wavelet power spectrum of the current at VKH; b) wavelet power spectrum of the current at LKH.

It highlights the need to analyze parts of a signal with high and medium GICs separately.

Numerous studies have shown that the GIC fluctuations have maximum values at certain frequencies, which are within the range of 1.5 to 8 mHz. This is confirmed by the results obtained above for four events, caused by GMDs. Pc5/Pi3 pulsations have a similar frequency range and may cause intense GICs [*Yagova et al.*, 2021]. This statement is also consistent with the results of the analysis, carried out in the paper. High GIC values were registered at frequencies that correspond to frequencies of Pc5/Pi3 pulsations.

The study of quasi-DC currents at two substations of the monitoring system allowed comparison of the power system responses at different points of it during geomagnetic storm. On the basis of the comparison of the maximum GIC values (Table 2), recorded during the geomagnetic storms of Solar Cycle 24, the following conclusion was reached. The topology of outgoing power lines has a significant impact on the GIC amplitude at the substation. If the outgoing and incoming lines are located in one direction (LKH), then incoming and outgoing quasi-DC currents are almost equal to each over, which makes the total current of the neutral close to zero. For this reason, even during strong geomagnetic storms, the values at the LKH substation rarely exceeded 7 A. And the measurement at the VKH substation, where the lines change their direction, on the contrary, had high values of quasi-DC currents.

4 Conclusions

Geomagnetically induced currents flowing in extended electrical networks may affect their normal operation. These currents are the result of the interaction between solar wind, directly related to solar activity, and Earth's magnetosphere. As stated previously in the paper, GICs are non-stationary signals, frequencies of which are close to zero and do not exceed 100 mHz. Well-known method of continuous wavelet transform was chosen for their detailed analysis. The method allows the determination of the frequency composition of a signal in time with sufficient accuracy.

The main results of the analysis presented in the paper are as follows:

1. The frequency range of 1.5–3.6 mHz of the analyzed GICs coincides with the frequency

range of Pc5/Pi3 pulsations. It is at these frequencies, the maximum GIC values were recorded.

2. There are no constant frequencies on the obtained scalograms of quasi-DC currents.

3. The scalograms, obtained as a result of the continuous wavelet transform of the GIC signal, corresponds well to the GICs fluctuations.

4. Study of the GIC signal with parts that have a large range of amplitudes does not provide clear results about frequency content of GIC at lower amplitudes.

5. The topology of the power lines at the studied substation strongly affects the GIC value.

Acknowledgments. This study is supported by the grant no. 22-29-00413 from the Russian Science Foundation (https://rscf.ru/project/22-29-00413/). The GIC data are available at the website (http://eurisgic.ru/). We appreciate IMAGE for providing geomagnetic field data (http://www.ava.fmi.fi/image/).

References

Adhikari, B., N. Sapkota, S. Dahal, B. Bhattarai, K. Khanal, and N. P. Chapagain (2019), Spectral characteristic of geomagnetically induced current during geomagnetic storms by wavelet techniques, *Journal of Atmospheric and Solar-Terrestrial Physics*, *192*, 104,777, doi:10.1016/j.jastp.2018.01.020.

Aksenovich, T. V. (2020), Comparison of the Use of Wavelet Transform and Short-Time Fourier Transform for the Study of Geomagnetically Induced Current in the Autotransformer Neutral, in *2020 International Multi-Conference on Industrial Engineering and Modern Technologies (FarEastCon)*, pp. 1–5, IEEE, doi:10.1109/fareastcon50210.2020.9271210.

Albert, D., P. Schachinger, R. L. Bailey, H. Renner, and G. Achleitner (2022), Analysis of Long-Term GIC Measurements in Transformers in Austria, *Space Weather*, *20*(1), e2021SW002,912, doi:10.1029/2021sw002912.

Barannik, M. B., A. N. Danilin, Y. V. Kat'kalov, V. V. Kolobov, Y. A. Sakharov, and V. N. Selivanov (2012), A system for recording geomagnetically induced currents in neutrals of power autotransformers, *Instruments and Experimental Techniques*, *55*(1), 110–115, doi:10.1134/s0020441211060121.

Belakhovsky, V., V. Pilipenko, M. Engebretson, Y. Sakharov, and V. Selivanov (2019), Impulsive disturbances of the geomagnetic field as a cause of induced currents of electric power lines, *Journal of Space Weather and Space Climate*, *9*, 18, doi:10.1051/swsc/2019015.

Boteler, D. H. (2001), Assessment of Geomagnetic Hazard to Power Systems in Canada, *Natural Hazards*, *23*(2), 101–120, doi:10.1023/A:1011194414259.

Choi, K.-C., M.-Y. Park, Y. Ryu, Y. Hong, J.-H. Yi, S.-W. Park, and J.-H. Kim (2015), Installation of Induced Current Measurement Systems in Substations and Analysis of GIC Data during Geomagnetic Storms, *Journal of Astronomy and Space Sciences*, *32*(4), 427–434, doi:10.5140/JASS.2015.32.4.427.

Dimmock, A. P., L. Rosenqvist, J.-O. Hall, A. Viljanen, E. Yordanova, I. Honkonen, M. André, and E. C. Sjöberg (2019), The GIC and Geomagnetic Response Over Fennoscandia to the 7–8 September 2017 Geomagnetic Storm, *Space Weather*, *17*(7), 989–1010, doi:10.1029/2018sw002132.

Erinmez, I., J. G. Kappenman, and W. A. Radasky (2002), Management of the geomagnetically induced current risks on the national grid company's electric power transmission system, *Journal of Atmospheric and Solar-Terrestrial Physics*, *64*(5–6), 743–756, doi:10.1016/s1364-6826(02)00036-6.

Falayi, E., O. Ogunmodimu, O. Bolaji, J. Ayanda, and O. Ojoniyi (2017), Investigation of geomagnetic induced current at high latitude during the storm-time variation, *NRIAG Journal of Astronomy and Geophysics*, *6*(1), 131–140, doi:10.1016/j.nrjag.2017.04.010.

Guillon, S., P. Toner, L. Gibson, and D. Boteler (2016), A Colorful Blackout: The Havoc Caused by Auroral Electrojet Generated Magnetic Field Variations in 1989, *IEEE Power and Energy Magazine*, *14*(6), 59–71, doi:10.1109/MPE.2016.2591760.

Kappenman, J. (2018), Geomagnetic Disturbances and Impacts upon Power System Operation, in *Electric Power Generation, Transmission, and Distribution: The Electric Power Engineering Handbook*, pp. 1–22, CRC Press, doi:10.1201/9781315222424-17.

Lee, G., R. Gommers, F. Waselewski, K. Wohlfahrt, and A. O'Leary (2019), PyWavelets: A Python package for wavelet analysis, *Journal of Open Source Software*, *4*(36), 1237, doi:10.21105/joss.01237.

Liu, C., L. Liu, and R. Pirjola (2009), Geomagnetically induced currents in the high-voltage power grid in China, *IEEE Transactions on Power Delivery*, *24*(4), 2368–2374, doi:10.1109/TPWRD.2009.2028490.

Mac Manus, D., C. Rodger, M. Dalzell, A. Thomson, M. Clilverd, and T. Petersen (2017), Long-term geomagnetically induced current observations in New Zealand: Earth return corrections and geomagnetic field driver, *Space Weather*, *15*(8), 1020–1038, doi:10.1002/2017SW001635.

Mallat, S. (2008), *A Wavelet Tour of Signal Processing: The Sparse Way*, 1–805 pp., Elsevier, doi:10.1016/B978-0-12-374370-1.X0001-8.

Molinski, T. (2002), Why utilities respect geomagnetically induced currents, *Journal of Atmospheric and Solar-Terrestrial Physics*, *64*(16), 1765–1778, doi:10.1016/S1364-6826(02)00126-8.

Oliveira, D., and C. Ngwira (2017), Geomagnetically Induced Currents: Principles, *Braz J Phys*, *47*, 552–560, doi:10.1007/s13538-017-0523-y.

Pulkkinen, A., S. Lindahl, A. Viljanen, and R. Pirjola (2005), Geomagnetic storm of 29–31 October 2003: Geomagnetically induced currents and their relation to problems in the Swedish high-voltage power transmission system, *Space Weather*, *3*(8), 08 03, doi:10.1029/2004SW000123.

Pulkkinen, A., R. Pirjola, and A. Viljanen (2008), Statistics of extreme geomagnetically induced current events, *Space Weather*, *6*(7), 07,001, doi:10.1029/2008SW000388.

Torrence, C., and G. P. Compo (1998), A Practical Guide to Wavelet Analysis, *Bulletin of the American Meteorological Society*, *79*(1), 61–78, doi:10/bhbwhf.

Trichtchenko, L. (2021), Frequency Considerations in GIC Applications, *Space Weather*, *19*(8), 2020 002,694, doi:10.1029/2020SW002694.

Viljanen, A. (2011), European Project to Improve Models of Geomagnetically Induced Currents, *Space Weather*, *9*(7), 07,007, doi:10.1029/2011SW000680.

Watari, S. (2017), Geomagnetic storms of cycle 24 and their solar sources, *Earth, Planets and Space*, *69*(1), 1–8, doi:10.1186/s40623-017-0653-z.

Watari, S., S. Nakamura, and Y. Ebihara (2021), Measurement of geomagnetically induced current (GIC) around Tokyo, Japan, *Earth, Planets and Space*, *73*(1), 102, doi:10.1186/s40623-021-01422-3.

Wik, M., A. Viljanen, R. Pirjola, A. Pulkkinen, P. Wintoft, and H. Lundstedt (2008), Calculation of geomagnetically induced currents in the 400 kV power grid in southern Sweden, *Space Weather*, *6*(7), doi:10.1029/2007SW000343.

Wu, C.-C., K. Liou, R. P. Lepping, L. Hutting, S. Plunkett, R. A. Howard, and D. Socker (2016), The first super geomagnetic storm of solar cycle 24: "The St. Patrick's day event (17 March 2015)", *Earth, Planets and Space*, *68*(1), 1–12, doi:10.1186/s40623-016-0525-y.

Xu, W.-H., Z.-Y. Xing, N. Balan, L.-K. Liang, Y.-L. Wang, and Q.-H. Zhang (2022), Spectral analysis of geomagnetically induced current and local magnetic field during the 17 March 2013 geomagnetic storm, *Advances in Space Research*, *69*(9), 3417–3425, doi:10.1016/j.asr.2022.02.025.

Yagova, N. V., V. A. Pilipenko, Y. A. Sakharov, and V. N. Selivanov (2021), Spatial scale of geomagnetic Pc5/Pi3 pulsations as a factor of their efficiency in generation of geomagnetically induced currents, *Earth, Planets and Space*, *73*(1), 1–13, doi:10.1186/s40623-021-01407-2.